Colloids and Surfaces B: Biointerfaces 245 (2025) 114281

Contents lists available at ScienceDirect

Colloids and Surfaces B: Biointerfaces

journal homepage: www.elsevier.com/locate/colsurfb

Hevea brasiliensis rubber particles' fluid interfaces reveal size impact on early coagulation steps

Marion Baudoin [a,b,c], Gilles Paboeuf [a,d], Siriluck Liengprayoon [e], Natedao Musigamart [e], Céline Bottier [b,c], Véronique Vié [a,d,*]

[a] IPR – UMR UR1 CNRS 6251, Rennes University, Rennes F-35000, France
[b] CIRAD, UPR BioWooEB, Montpellier F-34398, France
[c] BioWooEB, Univ Montpellier, CIRAD, Montpellier, France
[d] ScanMAT – UAR 2025, Rennes University, Rennes F-35042, France
[e] KAPI, Kasetsart University, Bangkok 10900, Thailand

ARTICLE INFO

Keywords:
Hevea brasiliensis latex
Small rubber particles (SRP)
Large rubber particles (LRP)
Particle size distribution
Langmuir film
Interfacial behavior
Atomic force microscopy (AFM)
Ellipsometry
Confocal laser scanning microscopy (CLSM)

ABSTRACT

Natural rubber originates from the coagulation of rubber particles (RP) from *Hevea brasiliensis* latex. The size distribution of *Hevea* RP is bimodal with the presence of small rubber particles (SRP) and large rubber particles (LRP). This study aims at getting a better understanding of the early coagulation steps of *Hevea* RP taking into account the particle size. SRP and LRP were obtained by centrifugation of freshly tapped ammonia-free latex from RRIM600 clone. Size and zeta potential measurements showed that both RP fractions were efficiently separated and stable in basic buffer. SRP and LRP dispersions were placed in a Langmuir trough and RP were let to adsorb at the air-liquid interface to form interfacial films. Surface tension and ellipsometry indicate that the formation kinetics and the stabilization of the film at the air-liquid interface are faster for SRP than LRP. Moreover, the arrangement of RP at the interface differs between SRP and LRP, as shown by Brewster angle microscopy, atomic force microscopy and confocal laser scanning microscopy. First, the RP membrane and *cis*-1,4-polyisoprene core spread at the air-liquid interface before clustering. Then, while the SRP fuse, the LRP keep their structure in individual particles in floating aggregate. The role of the non-isoprene molecules on the different organization of SRP and LRP films is discussed, the one of the two major RP proteins, SRPP1 (Small Rubber Particle Protein) and Rubber Elongation Factor (REF1) in the early coagulation steps.

1. Introduction

Latex collected from *Hevea brasiliensis* tree is the only commercial source of natural rubber (NR), the *cis*-1,4-polyisoprene polymer, a strategic raw material especially for automotive, medical and consumer applications. In 2022, the global NR production reached 14.6 million tons whose 36 % was produced by Thailand, the world leader in NR production [1]. Thailand produces several NR grades including concentrated latex whose production is approximately 1 million tons per year. Concentrated latex is obtained by centrifugation of field latex to increase its dry rubber content (DRC) from about 30–60 %. The rejected liquid from centrifugation is called skim latex and still contains 4–8 % DRC [2].

Latex is the cytoplasm of laticiferous cells [3], which are anastomosed to form vessels arranged in concentric rings in the phloem [4], and specialized in the synthesis of *cis*-1,4-polyisoprene. Due to the high turgor pressure in vessels, latex spontaneously exudes from *Hevea* tree after tapping, an operation which consists in doing a small incision in the bark to sever laticiferous cells. This feature of laticifers is exploited commercially to collect latex and manufacture NR. Freshly tapped *Hevea* latex appears as a white opaque fluid and contains approximately 60 % water, 35 % *cis*-1,4-polyisoprene polymer chains and 5 % non-isoprene molecules (proteins, lipids, carbohydrates and minerals) [5,6]. *Hevea* latex is a colloidal dispersion where various micrometric objects, mainly rubber particles (RP), lutoids and Frey-Wyssling particles, are dispersed in the cytoplasmic serum (C-serum) [7–9]. At this stage, the *cis*-1,4-polyisoprene polymer chains are only stored within spherical RP described as a hydrophobic *cis*-1,4-polyisoprene core surrounded by a monolayer membrane of lipids and proteins [10–13]. NR arises from the coagulation of RP [14]. This mechanism, essential, is still poorly

* Corresponding author at: IPR – UMR UR1 CNRS 6251, Rennes University, Rennes F-35000, France.
E-mail address: veronique.vie@univ-rennes.fr (V. Vié).

https://doi.org/10.1016/j.colsurfb.2024.114281
Received 29 May 2024; Received in revised form 25 September 2024; Accepted 27 September 2024
Available online 30 September 2024

understood nowadays. A better understanding of this mechanism could help to improve the quality of NR.

Interestingly, RP of *Hevea* latex exhibit a bimodal size distribution with the presence of small rubber particles (SRP, diameter ~ 0.05–0.4 μm) and large rubber particles (LRP, diameter ~ 0.4–3.0 μm) [15–18]. This bimodal size distribution has a direct consequence in the industry of concentrated latex. Indeed, after centrifugation of the latex, concentrated latex mainly contains LRP while skim latex mainly contains SRP [19,20]. The skim latex must be doped with huge amount of sulfuric acid to coagulate these SRP and make a by-product called skim rubber [21,22]. Although skim rubber is a lower-quality byproduct; it still generates a substantial income for concentrated latex factories. However, the important amount of sulfuric acid required to coagulate SRP and to produce skim rubber results in air and water pollutions which are detrimental for nearby communities and environment [23].

SRP and LRP represent, respectively, 94 % and 6 % of the total population of *Hevea* latex RP; and respectively, 7 % and 93 % of the total volume of RP [24]. In addition to their size difference, the biochemical compositions of SRP and LRP differ. Indeed, LRP contain both long and short *cis*-1,4-polyisoprene chains, while SRP comprise mainly long chains [17,25]. The membrane composition of SRP and LRP also exhibits differences regarding the nature and the contents of lipids and proteins. For instance, for RRIM600 clone, SRP display an equivalent proportion of phospholipids, glycolipids and neutral lipids, while in LRP, neutral lipids are ~3–4 times more abundant than phospholipids and glycolipids [26]. Protein expression varies in both SRP and LRP populations [27]. The two major proteins located at the RP membrane are rubber elongation factor (REF1, 138 amino acids, 14.6 kDa) [28] and small rubber particle protein (SRPP1, 204 amino acids, 22.4 kDa) [29]. Whereas REF1 is detected in both SRP and LRP membranes, SRPP1 is present only in SRP membrane [30]. Both REF1 and SRPP1 are suspected to play a significant role in the biosynthesis *cis*-1,4-polyisoprene [31–33].

Recently, several authors suggested that the mixing ratios of LRP and SRP contents could be tunable to improve desirable properties of rubber products of interest or to target specific applications. Indeed, it was shown that the size of RP from ammonia-stabilized *Hevea* latex influences various properties of NR samples manufactured from LRP, SRP and controlled mixtures of both RP fractions. For instance, the RP size impacts the process formation of dry particle films [34,35], as well as the mechanical properties of NR [36], of NR filled with carbon black [37] and of vulcanized NR samples [20,25]. These studies were realized with ammonia, a commonly used stabilizer shown to rapidly affect the biochemical composition of latex [31,32,38,39]. Rippel *et al.* used ammonia-free latex to prepare SRP and LRP thick films and also observed that the RP size impacts their colloidal properties as well as their coalescence and film formation [40]. Nevertheless, the drying of films, as used in this study, was shown to result in rearrangement and deformation of RP [35].

In this context, the present study was conducted on SRP and LRP in their hydrated state without ammonia, *i.e.* as close as possible as their native state when they exude from the tree. We used a Langmuir trough to form thin film at the air-liquid interface subjected to several characterizations [41]. W. G. Wren was the first, in 1942, to apply the Langmuir method to study films of ammoniated *Hevea* latex dropped at the air-liquid interface [42]. The method was later applied to characterize synthetic lattices [43–46]. The Langmuir method presents several advantages, *e.g.* its simplicity to implement and the possibility to combine complementary biophysical tools to investigate interactions between molecules or biocolloids at the air-liquid interface from animal or vegetable organisms [47–50]. More recently, this approach was applied to mimic the lipid-protein monolayer membrane of *Hevea* RP and the results showed that recombinant REF1 and SRPP1 proteins present different auto-assembling [51] and that they interact differently with model membranes made of synthetic lipids [52] and native lipids of *Hevea* latex [53].

In this work, the air-liquid interface was used to destabilize the RP coming from the bulk solution in order to get insight on the first step of coagulation. For this purpose, ammonia-free freshly tapped latex was used to extract the SRP and LRP fractions. The good separation of the two RP fractions by latex centrifugation and the stability of RP dispersions in basic buffer was checked by nanoparticle tracking analysis (NTA) and zeta potential measurements. To get information either the RP size governs the formation kinetics and the organization of the interfacial films, the adsorption of SRP and LRP at the interface was monitored by surface tension and ellipsometric measurements. These experiments provide information on lateral interactions and the amount of matter at the interface. Moreover, they were supplemented by Brewster angle microscopy (BAM) to observe the interfacial formation of films at the micrometer scale. The Langmuir-Blodgett methodology was used to transfer RP films from the air-buffer interface to a solid substrate and were observed by atomic force microscopy (AFM) at nanometer scale. In addition, fluorescent dyes were used to observe the localization of lipids and *cis*-1,4-polyisoprene in RP (solution and dry films) by confocal laser scanning microscopy (CLSM). Our results indicate that LRP and SRP thin films display different interfacial properties (adsorption time, lateral interactions) and different state of particle coalescence at the air-liquid interface and on solid substrate. This work complements previous studies by providing new insights into the behavior of hydrated LRP and SRP films and then validates assumptions previously formulated in the literature.

2. Materials and methods

2.1. Collection of latex and separation of RP according to their size

Latex was collected from ten regularly tapped *Hevea brasiliensis* trees of RRIM600 clone at a plantation of Visahakit Thai Rubber Co., Ltd., Chanthaburi, Thailand. The trees were tapped in early morning (5 a.m.). One hour later, latex that dropped in a clean plastic cup placed on ice (4 °C) was collected. The lattices from the 10 trees were poured in a glass bottle which was stored in ice until arrival in the laboratory (Bangkok.).

The two centrifugation fractions of *Hevea brasiliensis* latex containing large rubber particles (LRP) and small rubber particles (SRP) were obtained by applying the 2 first steps of the 4-steps centrifugation method previously described [26]. Briefly, the whole latex was first centrifuged at 16,000 g for 45 min at 4 °C (centrifugation C1). This low centrifugal force prevents RP from coagulating. Moreover, it allows a proper separation of RP according to their sizes as LRP concentrate at the top of the centrifugation tube while SRP remain suspended in the C-Serum. After C1 centrifugation, LRP were collected with a spatula, while the C-serum containing SRP in suspension was sucked with a syringe. To separate the SRP from the C-serum, the C-serum containing SRP was centrifuged a second time at 45,000 g for 45 min at 4 °C (centrifugation C2). After separation, LRP and SRP were dispersed in a buffer (Tris 100 mM, pH 10) at a concentration of 10 mg mL^{-1} and the obtained suspensions were stored at 4 °C throughout the study. The stability of particles in solution was checked by Turbiscan measurements carried out once a month. In addition, particle size measurements by NTA were also carried out at the beginning and the end of this study to validate that there was no aggregation nor coalescence of particles in the stock solution during all the study (technical details of NTA are presented in paragraph 2.2 and results in supplementary data).

2.2. Nanoparticles tracking analysis (NTA)

The size distribution of SRP and LRP dispersions was measured by Nanoparticle Tracking Analysis (NTA), specifically by a NanoSight LM10 (Malvern Instruments, Malvern, UK). SRP and LRP dispersions were diluted in a buffer (Tris 100 mM, pH 10) at a concentration of 0.02 mg mL^{-1} before being placed in the instrument cell. Measurements were made on three 30 s video captures per sample with a 638 nm laser

beam and at 25 °C. Videos were recorded with a CCD camera and then analyzed to follow the trajectory particles and calculate their diameter using the NanoSight NTA 3.1 software (Malvern, UK). The curves presented in supplementary data are the average of these three simultaneous measurements, expressed as a percentage of particles per sample as a function of diameter. This particle size analysis was used to verify the stability of the dispersions over time. Indeed, no coagulation nor creaming was observed during all the experiments (data not shown).

2.3. ζ-potential measurement

The stability of the dispersions studied depends on the distribution of charges on the surfaces of the suspended RP and the electrostatic interactions between them. The zeta potential allows measuring the electrical surface tension resulting from these interactions and thus to determine if the dispersion is stable or if aggregates are formed. To measure the Zeta potential of dispersion diluted at 0.02 mg mL^{-1} in Tris Buffer (100 mM, pH10), we used a sample capillary cell (DT1070) and a zeta potential analyzer (Malvern Nanosizer). Zeta potential measurement was made at 25 °C for 1 minute. Each measurement was performed in triplicates.

2.4. Ellipsometry and surface pressure measurements

Interfacial film formation is characterized by ellipsometric angle and surface pressure measurements over time. The ellipsometric angle (Δ, °) measurements were performed using a home-made ellipsometer in null configuration, equipped with a polarized He-Ne laser (wavelength 632 nm). The ellipsometric angle is related to two parameters which are the reflective index and the thickness of the interfacial film. Usually, the ellipsometric angle is correlated to the amount of matter at the interface. The laser has a surface area of 1 mm^2 and probes a depth of 1 μm. The accuracy of the delta angle measurement is 0.2 ° [54]. The surface pressure (π, mN m^{-1}) was measured by the Wilhelmy method using a filter paper plate connected to a microelectronic feedback system (Nima Technology, UK). The accuracy of surface pressure measurements is 0.5 mN m^{-1} [54].

All ellipsometric angles and surface pressures were recorded simultaneously as function of time at room temperature varying in the range 19–21°C. Different sizes of trough were used depending on the experiment carried. In all cases, the cleanness of the interface was checked by performing measures on the ultrapure water and on the buffer for 5 minutes or under compression. Without ellipsometric angle evolution nor surface pressure variation, the initial values of both parameters are considered as references and equal to zero. Then the rubber particle dispersions (0.6 mg mL^{-1}) are directly placed in the trough just after dilution from the stock solution (10 mg mL^{-1}). As the experiment is performed on long kinetics (>20 h), the evaporation phenomenon was compensated by using an automatic syringe pump which regularly injects water to insure a constant volume. The curves presented on the paper are representative of at least two experiments.

2.5. Brewster angle microscopy (BAM)

Brewster angle microscopy (BAM) is a microscopy method providing a direct visualization of the air-liquid interface (Nanofilm EP3, Accurion, DE). The 532 nm laser beam is reflected by the interface with the Brewster angle $\theta_{Brewster}$ to the 10x objective and CCD detector to generate images. The Brewster angle, is defined by the Fresnel equation:

$$\theta_{Brewster} = \arctan(n_{water}/n_{air})$$

with n_{water} and n_{air} the refractive indices of water and air, respectively. The value of the $\theta_{Brewster}$ is 53.1 °. At this angle, the incident laser polarized p (parallel to the plane of incidence) is perfectly transmitted through the interface, without reflection. So, on pure water, we obtain an image of the interface with a minimal light intensity. When RP are adsorbed at the air-liquid interface, the refractive index differs from that of water, light is partially reflected and the level of gray increases in the image. In other words, the level of gray depends on the density of matter at the interface. As for the ellipsometry and surface pressure measurements, the samples are directly placed in the trough after dilution at 0.6 mg mL^{-1}. To compensate for the evaporation phenomenon, water is injected in the trough during all the experiment thanks to an automatic programable syringe pump. The experiments were carried out on 20 hours kinetics at room temperature which can vary in the range of 19 °C-21 °C.

2.6. Atomic force microscopy (AFM)

The organization of the interfacial film at a molecular scale, and at higher resolution than the BAM, was obtained with atomic force microscopy. For this purpose, the interfacial film was transferred to a mica plate by the Langmuir-Blodgett method. Then, a new 50 mL trough equipped with movable barriers, was used and placed on the ellipsometric and tensiometric setup that allowed to control, for each transfer, the values of delta angle and surface pressure. Indeed, the transfers were performed at selected values of Δ and π determined from the previous absorption kinetics.

After transfer to the solid substrate, the sample remains at a temperature ranging from 19°C-21°C. The sample was imaged 24 h later. The interfacial RP films were imaged by AFM (Multimode Nanoscope 8, Bruker, France), using the PeakForce Quantitative Nanomechanical Mapping (QNM in air) mode. This mode provides a high-resolution topography of the sample surface at the nanoscale, without degradation, and allows to obtain images in height variation and in deformation. All the images were obtained with a standard silicon cantilever (0.06 N m^{-1}, SNL-10, Bruker, France), a scan rate fixed at 1 Hz and an image resolution of 512×512 pixels. The AFM images in height variation and deformation were analyzed using the Gwyddion software (2.55). The color scales were provided to facilitate the interpretation of the images.

2.7. Confocal laser scanning microscopy (CLSM)

The structure of RP in solution and in film was observed using a confocal laser scanning microscopy (CLSM) system (Leica SP8, Heidelberg, Germany). This inverted microscope is equipped with an argon laser (excitation at 488 nm) and two He-Ne lasers (excitation at 543 and 633 nm). The wide excitation range enables images to be taken by exciting samples at the correct wavelength to collect the light emitted from the dyes. For all images, a 64x oil-immersion objective was used. For the labelling of the different components of the RP, two fluorescent markers were used [55,56], *i.e.* Lipidtox to visualize *cis*-1,4-polyisoprene (0. 2:100, v/v, λ_{ex} = 488 nm - λ_{em} = 590 nm, Invitrogen) and Rd-DOPE to visualize polar lipids (1:100, v/v, 16:0 Liss Rhod PE 1,2-dioleoyl-sn--glycero-3-phosphoethanolamin-N-(lissamin rhodamin B sulfonyl), λ_{ex} = 543 nm - λ_{em} = 590 nm, Avanti Polar Lipids). The two markers were added to samples in solution 10 minutes before observations, and a 20 μL drop of RP solution was then placed on a glass slide. For dry film samples, a 25 μL drop of RP labelled solution was spread on a plasma-cleaned glass slide 24 hours before observation.

3. Results and discussions

3.1. Both RP fractions are efficiently separated by centrifugation of fresh latex and are stable in basic buffer

Ammonia-free fresh latex from *Hevea brasiliensis* was centrifuged to isolate both SRP and LRP fractions which were stabilized as highly-diluted dispersions (0.02 mg mL^{-1}) in a basic buffer (Tris 100 mM, pH 10). These dispersions were characterized by measuring their size distribution and zeta potential (Table 1). The size distributions of SRP and LRP obtained by NTA, are centered on very contrasting diameters which

Table 1
Particle size and zeta potential of SRP and LRP.

Fraction	Diameter [nm]	ζ-potential [mV]
SRP	141; 187	−66 ± 2
LRP	575; 637	−72 ± 1

± stands for calculated standard deviation on 3 duplicated measurements.

reflects a good separation of the two RP fractions. Indeed, NTA provides the particle concentration and their diameter thanks the particle diffusion in solution. Given that both SRP and LRP dispersions were prepared at the same mass concentration, the maximal value of the SRP peak has a particle concentration (2.5×10^7 particles/mL) about 10 times higher than the maximal value of LRP peak (2.5×10^6 particles/mL) (data shown in supplementary data).The size distribution of SRP shows a nearly unimodal distribution with a very thin and intense peak, at a diameter of 141 nm, maximum obtained by a gaussian fit; and a small shoulder, at a diameter of 187 nm, whose intensity is 5.5 times lower than the first one. In contrast, the size distribution of LRP shows a broad peak centered at a diameter of 575 nm, as well as a shoulder at a diameter of 637 nm, whose intensity is twice as low as the first one. The measured diameters for both SRP and LRP (Table 1) are in the same range as the ones reported in the literature [16,18,20].

The physical stability of RP dispersions was evaluated through zeta potential which is a usual indicator of particle repulsion. Indeed, repulsion between RP should be high enough to limit aggregation, coagulation or creaming. The zeta potential measured at basic pH are –66 ± 2 mV and –72 ± 1 mV for SRP and LRP, respectively. These values are consistent with the ones measured by Rippel *et al.* on ammonia-free RP dispersions in 10^{-3} mol.l^{-1} KCL solution: –70 and –64 mV for LRP and SRP, [40]. These absolute values higher than ± 30 mV reflect a good repulsion between RP, as well as a good stability of RP dispersions, although no ammonia was added [57]. These high values result from the negatively charged membrane which surrounds the polymeric core of natural latex particles [19,31,58]. This membrane is made up of negatively charged proteins having isoelectric points ranging from 3.9 to 4.6 [27,59,60].

RP solutions were imaged by confocal laser scanning microscopy (CLSM) using selective fluorescent probes to localize polar lipids and hydrophobic *cis*-1,4-polyisoprene chains. This method was only used on LRP. A correct visualization of individual SRP was difficult because of their high mobility in solution. On the confocal micrographs of the LRP shown in Fig. 1, the core/shell structure proposed by Siler *et al.* is observed [12]. The association of the two fluorescent probes (Fig. 1, image C) shows individual RP with a green core composed of hydrophobic *cis*-1,4-polyisoprene chains (seen individually on Fig. 1, image B) surrounded by an orange membrane composed of polar lipids (seen individually on Fig. 1, image A). These observations validate the LRP structure described in the literature [10–13], but also indicate the integrity of the LRP membrane. The particle separation and stabilization process did not damage the LRP integrity for further experiments.

3.2. The formation and stabilization of the particle film at the air-liquid interface is faster for SRP than LRP

The film formation kinetic of SRP and LRP at the air-liquid interface was monitored on a Langmuir trough by surface pressure, ellipsometry and BAM measurements for 20 hours. These measurements provide information on the amount of material at the air-liquid interface and on the organization of the interfacial layer. Fig. 2**a** and Fig. 2**b** respectively show the curves of surface pressure π and ellipsometric angle Δ as a function of time, during the adsorption of SRP and LRP at the air-liquid interface. The evolution of the surface pressure over time is similar for both RP sizes (Fig. 2**a**). A rapid and regular increase is observed up to about 5 hours, followed by a net slowdown from 5 to 10 hours, and finally the appearance of a plateau at a maximum surface pressure value π_{max}. The increase in surface pressure over time reflects the RP affinity for the air-liquid interface [61]. Once the surface pressure has been reached, there is a slight decrease in surface pressure due to energy stabilization of the layer. Despite the similar general shape of the surface pressure, two major differences are observed between SRP and LRP. First, the slope of the curve within 0–5 hours is much steeper for SRP, as compared to LRP, reflecting a more rapid adsorption at the air-liquid interface of SRP, as compared to LRP. This difference in slope agrees with the theoretical diffusion coefficient calculated from the Stokes-Einstein law predicting a faster adsorption of SRP than LRP at the interface as their smaller size allows a faster diffusion in the liquid. Second, SRP reach their maximum pressure over a shorter time (10 hours) than LRP (16 hours), indicating a more rapid interface saturation and organization of the SRP layer.

The maximum surface pressure π_{max} of SRP is higher than the one of LRP: it reaches π_{max}=19.8 mN m^{-1} at 10 hours kinetics for SRP, while LRP have a π_{max}=14.3 mN m^{-1} at 16 hours kinetics. The higher maximum surface pressure values measured for SRP compared to LRP indicate stronger lateral interactions in the SRP film than in the LRP one. These lateral interactions could result from a more pronounced destructuration of SRP as compared to LRP. In fact, the hydrophobic-hydrophilic interface induces a destabilization of the particles, as compared to the bulk where they are completely surrounded by an aqueous environment. This SRP destabilization would result in the spreading of the RP membrane components and *cis*-1,4-polyisoprene chains at the interface, and consequently in an increase of lateral molecular interactions. In contrast, the surface pressures for LRP reached lower values than SRP indicating lower lateral interactions either because of different molecular species or lower number of molecules than SRP.

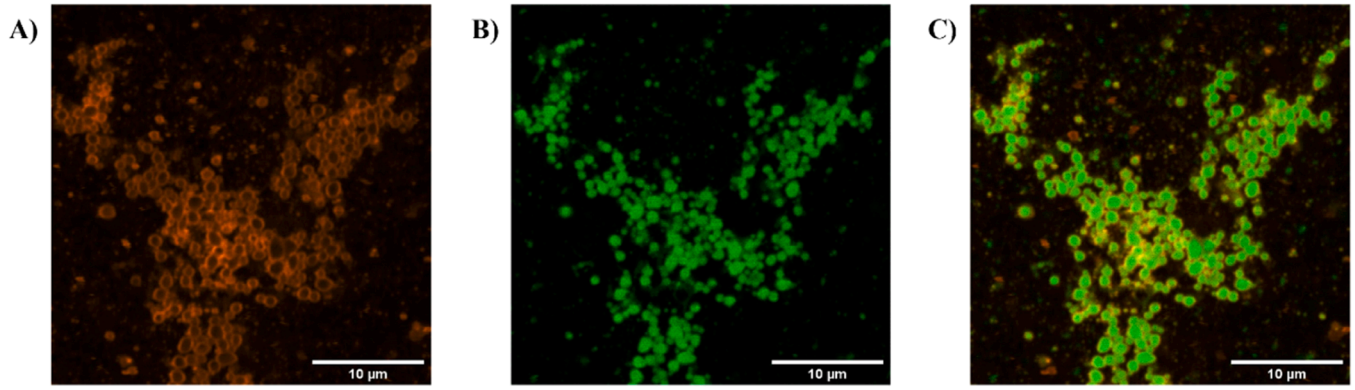

Fig. 1. CLSM images of LRP in Tris buffer, ×60 Zoom, with labelling of A) polar lipids in orange (Rhodamine-PE®), B) cis-1,4-polyisoprene chains in green (Lipidtox®) and C) merged image of A and B.

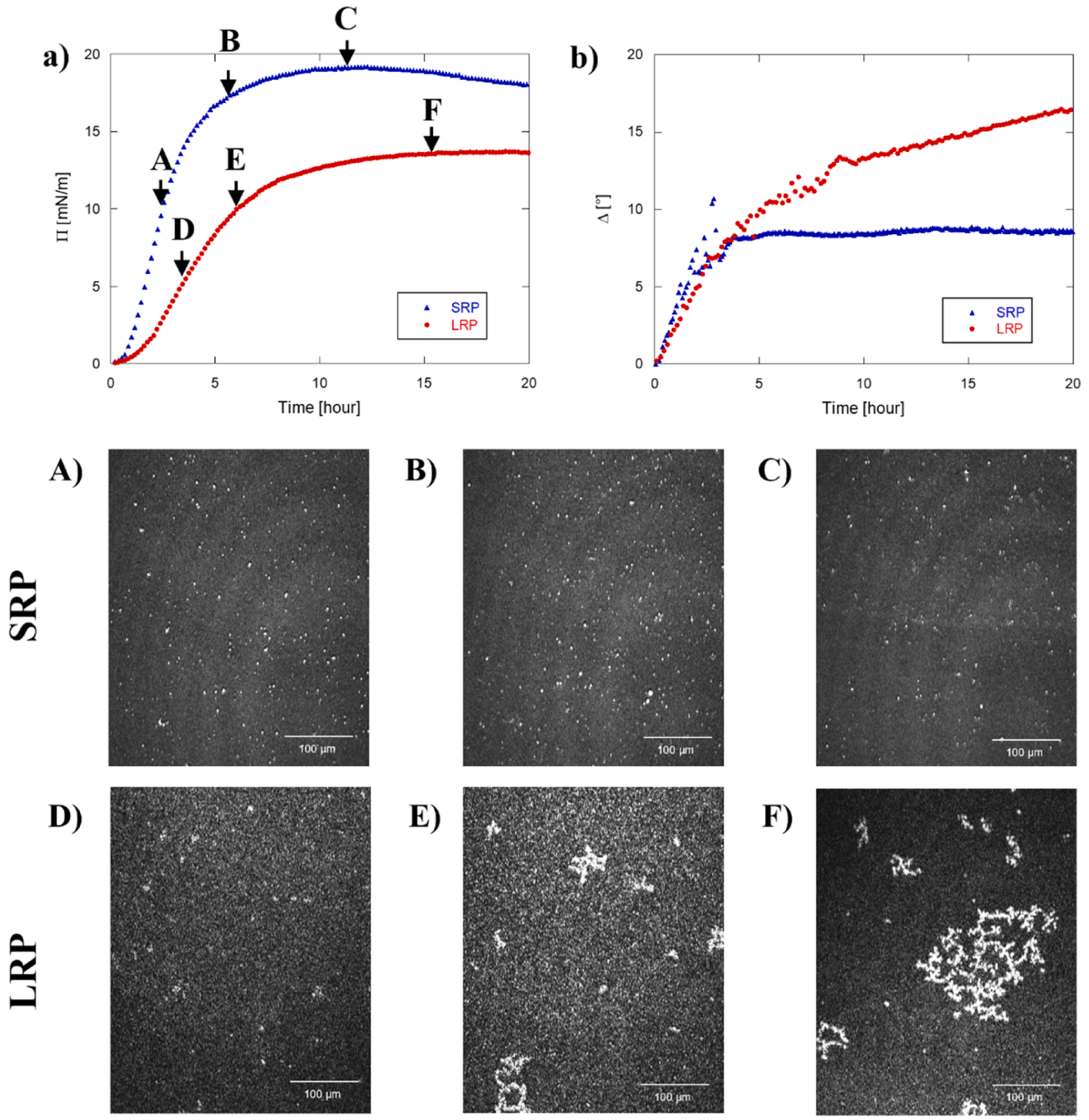

Fig. 2. Temporal evolution of surface pressure a) and ellipsometric angle b) during the 20 hours adsorption kinetic of SRP (blue triangles) and LRP (red circles) at the air-liquid interface. BAM images (395 ×494 µm^2) recorded at various times of the 20-hours adsorption kinetics of SRP (A-C) and LRP (D-F) at the air-liquid interface. Letters A-F correspond to the letters shown on graph a).

In contrast to the surface pressure, which evolves differently for the two RP fractions, the time course of the ellipsometric angle shown in Fig. 2**b**, indicates that, up to 4 hours, both adsorption kinetics of SRP and LRP are very similar. The two curves are almost superimposable indicating that the rate of material arrival at the interface is identical for both RP sizes. It is important to note that the ellipsometric angle is related to the presence of matter to a depth of 1 µm below the interface, which can explain the difference in the temporal detection between the surface pressure and the ellipsometric angle.

Although the surface pressure increases up to 10 hours for SRP (Fig. 2**a**), the ellipsometric angle exhibits a different kinetic. Indeed, the Δ value shows a noisy increase in the first 4 hours of the kinetics corresponding to the adsorption of SRP at the interface and its coverage. Beyond this time and until 20 hours, there is a stabilization of the ellipsometric angle at Δ=8.5°. This plateau indicates that the amount of matter at the interface does not evolve with time, meaning that there is a saturated layer at the air-liquid interface. Stable ellipsometric angle, in the period from 4 to 10 hours, associated with an increase of the surface pressure (from 15.8 mN m^{-1} to π_{max}=19.8 mN m^{-1}) indicates the development and the establishment of interactions within the interfacial layer. In summary, from 0 to 4 hours, the SRP film formed at the air-liquid interface regularly becomes denser until the amount of material

stabilizes. However, the SRP film continues to evolve and undergoes lateral interactions up to 10 hours kinetics, where the film reaches an equilibrium.

While the kinetics in ellipsometry are identical during the first 4 hours after deposition for both RP fractions, the ellipsometric angle of LRP does not behave in the same way as the one of SRP beyond this time. Unlike SRP, there is no stabilization of the LRP delta values, but a regular increase is observed instead, until a value of $\Delta = 20.1^{\circ}$ at 20 hours. The curve continues to increase, and this value doesn't seem to correspond at a plateau value. Indeed, a regular increase of the ellipsometric angle associated to a stable surface pressure is characteristic of increase of the thickness of the film, in accordance with the presence of matter under the interfacial layer over time. Furthermore, in contrast to SRP, the lower surface pressure (π_{max}=19.8 mN m^{-1} for SRP and π_{max}=14.3 mN m^{-1} for LRP) reflects weaker lateral interactions in the film which could suggest that most of the LRP particles keep their three-dimensional structure.

The direct and *in situ* visualization of the interface at the micrometer scale by BAM is shown in Fig. 2 to follow precisely the different stages of particle adsorption kinetics. The images A, B and C (letters defined in Fig. 2**a**) show the organization of SRP film at surface pressures of 10, 17 and 20 mN m^{-1}, respectively. At 10 mN m^{-1}, an increase in the overall gray level of the surface compared to that of the buffer can be observed and some bright spots appear at the interface. This variation in gray level

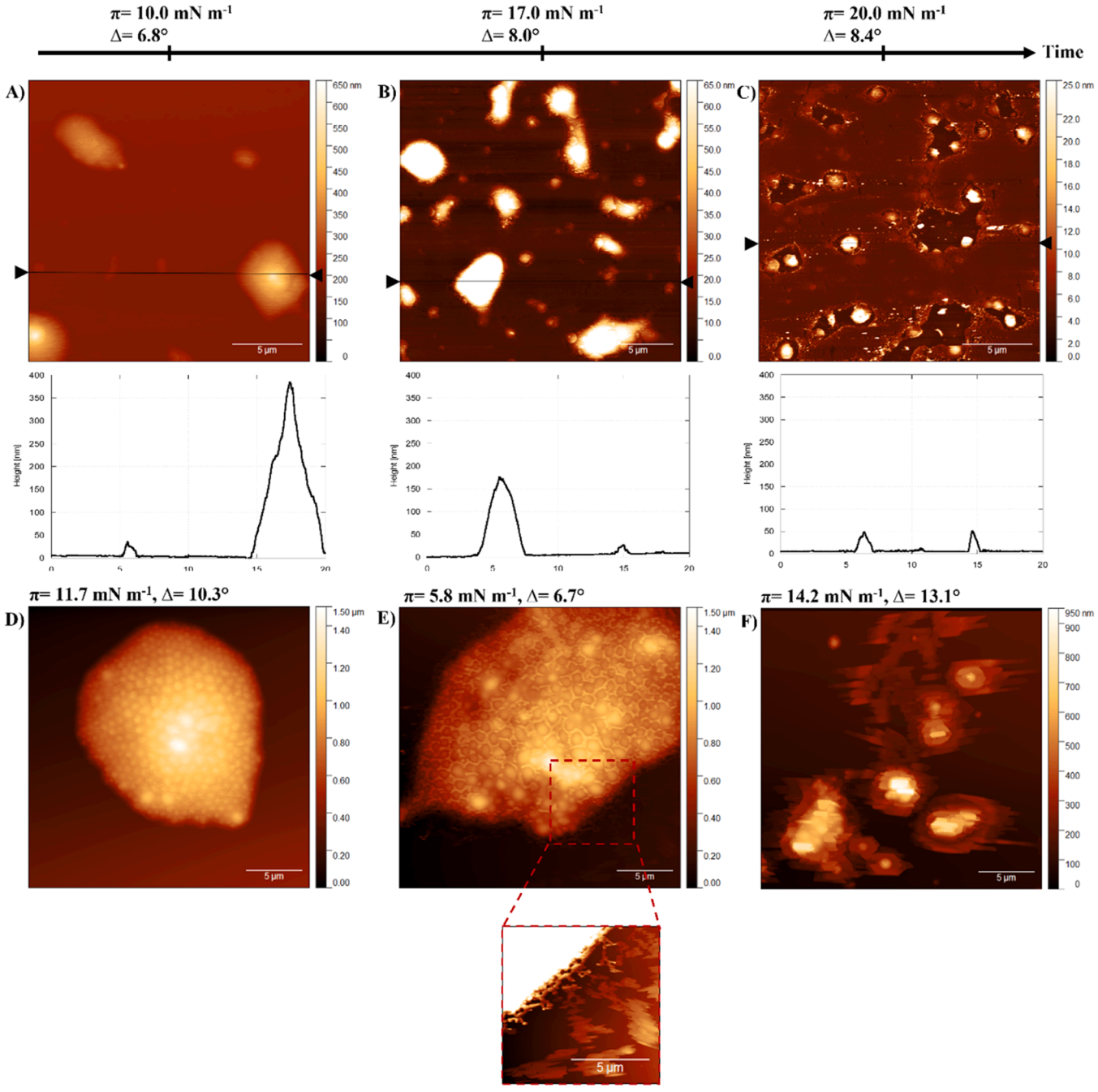

Fig. 3. Temporal evolution of AFM images in height mode (top) and profile sections of Langmuir-Blodgett films (bottom) of SRP (A to C) and (D to F) transferred on a solid substrate at various times of the adsorption kinetic. For each time, both surface pressure and ellipsometric angle are indicated. Letters A-F of this figure correspond to letters shown in Fig. 1a. The scale of the AFM images differs from ΔZ=650 nm, ΔZ=65 nm and ΔZ=25 nm for A, B, C and ΔZ=1,5 µm, ΔZ=1,5 µm and ΔZ=950 nm for D, E, F, respectively. The scale of the section graph for SRP images is the same for the three images ΔZ=400 nm respect to the image background.

corresponds to a change of the refractive index of the surface layer, the consequence of the presence of matter at the air-liquid interface. In addition, the appearance of white spots can be equated to the formation of aggregates at the interface. While the surface pressure increases, no evolution at the microscopic scale was detected between images A, B and C, in accordance with the stabilization of the ellipsometric angle. The bright spots at the interface do not show any evolution in size nor coalescence during the adsorption kinetic of SRP film.

Conversely, BAM images D, E and F (Fig. 2), taken at 5, 10 and 15 mN m^{-1} during the adsorption kinetic of LRP film, show a visible evolution of the interfacial organization. Indeed, when the surface pressure rises, the emergence of bright spots under form of clusters with irregular shapes was observed at the interface (Fig. 2, image D). These clusters increase in number along the time before regrouping to form larger domains of interconnected clusters (Fig. 2, images E and F). This clustering reflects the presence of attractive interactions contrary to the SRP, where no morphological evolution was visible during the kinetics. In addition, a noisy and sparkling background is observed, reflecting strong subphase activity for the LRP. This subphase activity could correspond to the presence of LRP under the interfacial layer over time, as deduced from surface tension and ellipsometry data.

Considering the results obtained with the various air-liquid interface characterization techniques, the interfacial film formation process differs according to particle size, with a spreading of molecular content of SPR more efficient than LRP. Moreover, the LRP film formation led to the appearance of aggregate networks. The role of the size is highlighted by these results, although it must be kept in mind that the RP size is related to specific biochemical composition.

3.3. *The RP membrane and cis-1,4-polyisoprene core of SRP spread at the air-liquid interface while LRP keep their structure in individual particles*

Atomic force microscopy allowed the characterization, at a higher resolution than BAM, of the interfacial film at the same surface pressures previously defined in Fig. 2**a**. Fig. 3 summarizes the height AFM images of SRP during the film formation (images A, B) and the stabilization stage of the kinetics (image C). Below each AFM image, the height profile graphs are plotted for a section represented by a black line on the images. Each height image in Fig. 3 is also presented in deformation mode in Fig. 4 (images A, B and C). Overall, the height images show a homogeneous distribution of light brown protrusions, with smooth and rounded edges, embedded in a darker background of low roughness. Although these protrusions do not have any specific shape nor specific values in height and lateral size, some general characteristics can be highlighted and will be discussed below as they undergo drastic changes during the formation of the SRP film.

At π =10 mN m^{-1}, (Fig. 3, image A), the protrusions observed at the interface display a maximum height relative to the background of 424 nm, whereas their lateral size reaches a maximum of 5.2 µm in diameter. The SRP in solution were previously shown to have a diameter of 141 nm, while the protrusions have much higher diameters and heights. Thus, it seems that the adsorption of individual SRP at the interface induces their aggregation, as well as a loss of their integrity, possibly induced by a molecular reorganization. The corresponding deformation image (Fig. 4, image A) highlights details that are not clearly visible in the height image due to the large range in color scale. These details reveal a heterogeneous background with the presence of areas displaying deformation values like the ones of the protrusions, suggesting the same chemical nature. Moreover, the surface of the protrusions also shows heterogeneous mechanical response assimilated to the height variation observed on the height image (Fig. 3, image A). This height variation is difficult to quantify because of the strong curvature of the protrusion. The highest zones of the protrusions are associated to lower deformation values which probably indicates that the chemical composition of protein and lipid of those zones differs from the rest of the protrusion, in agreement with the previously suggested molecular reorganization. The protrusions are embedded in a background which is itself composed of molecules, as evidenced by the increase in

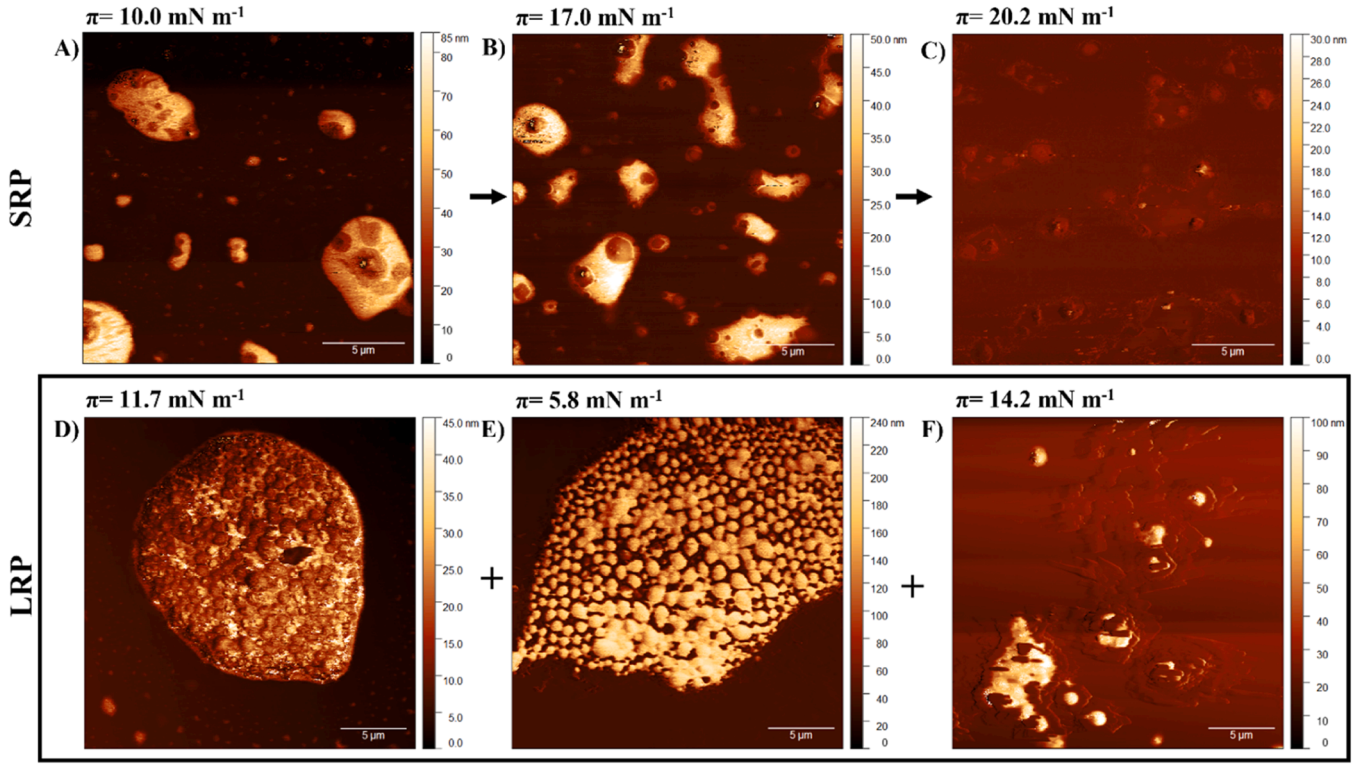

Fig. 4. AFM images in deformation mode of Langmuir-Blodgett films of SRP (A-C, corresponding to images A-C in Fig. 3) and LRP (D-F, corresponding to images D-F in Fig. 3).

surface pressure at the beginning of the kinetics (from $\pi = 0$ mN m^{-1} to 10 mN m^{-1}) indicating a lateral cohesion between molecules at the liquid/air interface. Although their nature is not yet determined, it is reasonable to think that this background is made of lipids and/or lipid/protein complexes arising from the lipoprotein membrane surrounding the hydrophobic *cis*-1,4-polyisoprene core of the SRP. In summary, while SRP are stable in a hydrophilic environment thanks to their core/shell structure, the hydrophilic/hydrophobic liquid/air interface leads to SRP destructuration. This phenomenon has already been observed on lipoproteins/oleosomes having similar structure as RP, *i.e.* hydrophobic core covered by a membrane, but with different chemical compositions (protein and lipid) [61,62]. In the case of SRP, the deformation heterogeneity observed on the surface of the aggregates suggests areas of different chemical compositions on the surface. This could result from the persistence of SRP membrane fragments.

At higher surface pressure (π = 17 mN m^{-1}), an increase in the number of protrusions in the interfacial film is observed in height image (Fig. 3, image B). The protrusions show the same surface heterogeneities, in both height and deformation (Fig. 4, image B), as those observed on the sample at π =10 mN.m^{-1} (images A in Fig. 3 and Fig. 4). These less deformable and higher areas are circular in shape regardless of the size of the protrusion. The main difference between the two surface pressures is the maximum apparent height of the protrusions which decreases from 424 nm to 263 nm when the surface pressure increases from 10 to 17 mN.m^{-1}. Moreover, the increase in surface pressure from 10 to 17 mN m^{-1} is accompanied by an increase in the ellipsometric angle (from 6.8 to 8°) indicating additional adsorption of SRP and form of aggregates during kinetics. This densification associated with the variation in the amount of material at the interface can be related to a thickening of the film caused by a partial spreading of the aggregates at the interface.

At the highest surface pressure ($\pi = 20$ mN.m^{-1}, Fig. 3, image C), the SRP film shows a totally different structure, as compared to images recorded at lower surface pressures (Fig. 3, images A and B). The image presents a background that is continuous and homogeneous in height, with the presence of height depressions of variable shapes. In these height depressions areas, circular protrusions appear with a maximum height of 60 nm and a width close to 1 μm. The deformation values of the sample are homogeneous (Fig. 4, image C). Contrary to both images recorded at lower surface pressures, the surface of the protrusions does not show any variation in height, nor variation in deformation. The AFM images of SRP show a disappearance of the aggregates, strongly suggesting the spreading of the *cis*-1,4-polyisoprene cores and SRP membrane components due to RP membrane disruption. The SRP lipoprotein membrane contains a major protein named SRPP1. According to Berthelot *et al.*, SRPP1 only binds to the lipid polar heads [52] and is easily released from the RP membrane [63], certainly favoring the destructuration of SRP when reaching the interface. Our observations can be related to the work of Rippel *et al.* [40] who observed by AFM a strong coalescence of thick and dense films formed by ammonia-free SRP. Indeed, our interfacial film characterization reveals the aggregation of SRP followed by coalescence and the first step of coagulation at the air-liquid interface.

CLSM was performed on SRP deposits, labelled with selective fluorescent probes for polar lipids and *cis*-1,4-polyisoprene hydrophobic chains. Fig. 5 gathers the confocal micrographs highlighting polar lipids in orange (image A), hydrophobic *cis*-1,4-polyisoprene chains in green (image B) and an assembly of the two probes (image C). These images do not show the topologies of individual particles, but aggregates without characteristic size, as visualized by AFM in the early stages of kinetics. The aggregates are composed mainly of hydrophobic chains in green (Fig. 5, image B), validating the hypothesis that the polymeric cores of individual SRP coalesce during particle adsorption at the air-liquid interface. Image A (Fig. 5) shows a layer of polar lipid dyes surrounding the aggregates. This lipid layer corresponds to the least deformable areas observed on AFM images of the interface in deformation mode

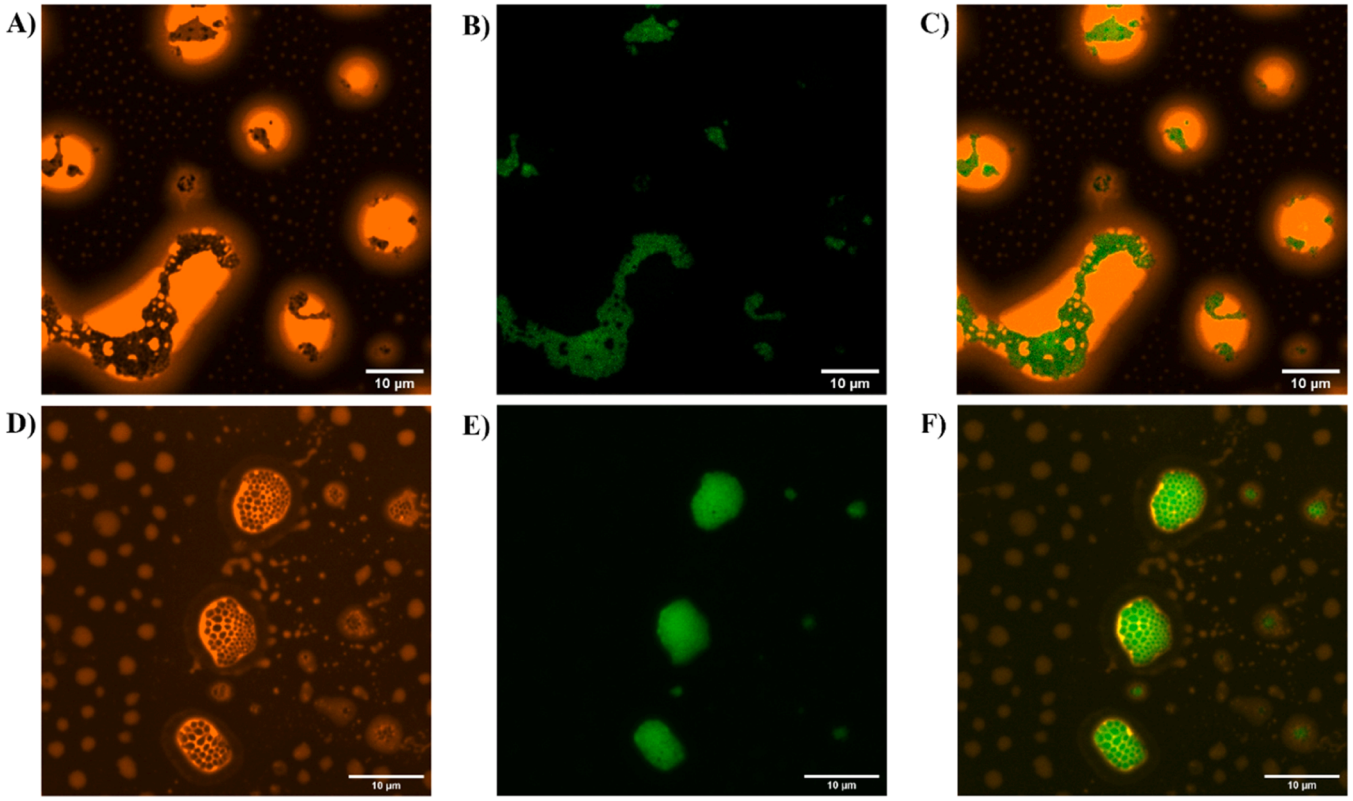

Fig. 5. CLSM images of SRP (A-C) and LRP (D-F) dry films, ×60 Zoom, with labelling of polar lipids in orange (Rhodamine-PE®) (A and D), cis-1,4 polyisoprene chains in green (Lipidtox®) (B and E) and merged images (C and F).

(Fig. 4, images A and B). More precisely, lipids are present with hydrophobic *cis*-1,4-polyisoprene chains. Some polar lipids, possibly phospholipids and/or glycolipids, remain bound to *cis*-1,4-polyisoprene chains. Confocal micrographs (Fig. 5, image C) reveal the destructuration of SRP at the interface, with coalescence of *cis*-1,4-polyisoprene hydrophobic cores and destabilization of the lipid/protein membrane. The lipid layers above the polymer chain aggregates show a strong response under light excitation. We can assume that the polar lipids constituting the SRP membrane will reorganize on the surface of the aggregates in the form of multilayers to ensure their stability in a hydrophobic environment although some lipids remain bound to *cis*-1,4-polyisoprene chains. The RhoPE inserted on polar lipid is also visible on the sample background. The presence of this lipid background confirms the formation of a continuous film at the interface.

In contrast to SRP, AFM images taken during the adsorption kinetics of LRP present three main structures shown in height and deformation modes in Fig. 3 (images D, E and F) and Fig. 4 (images D, E and F), respectively. These three interfacial organizations are present whatever the surface pression ($\pi = 5.8$ mN m^{-1}, 11.7 mN m^{-1} and 14.2 mN m^{-1}). Two of these observed structures (Fig. 3, images D and E) seem to result from individual LRP aggregation. In fact, each particle can be clearly distinguished in these structures of several micrometer in diameter. This phenomenon was previously observed by Rippel *et al.* [40] on ammonia-free LRP films, where RP were shown to retain their topology in individual particles. The measurement of the particle diameter (n=15 particles, image E) gives a mean value of 658 ± 109 nm. To avoid the edge effects on the measurement, only the particles of the center were considered. The height of these structures did not exceed 1 μm corresponding to the thickness of a single particle. The values of thickness and diameter measured in these AFM images are in accordance with size measurement of LRP in solution. Thus, it seems that the air/water interface induces a lateral attraction between LRP, without any coalescence of RP. This tri-dimensional structural stability can be related to the presence of the major protein of LRP, REF1, which penetrates deeply into the lipid monolayer [52]. The strong anchoring of REF1 protein in LRP membrane probably contributes to the fact that LRP keep their integrity once at the interface.

Although the height and diameter of the structures observed in images D and E (Fig. 3) are in the same range, some differences are shown in height and deformation images. Indeed, on image D (Fig. 3), the individual particles appear as beads in close packing. The height image presents depressions between RP. The image of deformation does not present high variation on the top of these structures (~25 nm of variations) suggesting homogeneous surface properties. In contrast, in Fig. 3 image E, the zone of separation between individual particles seems filled with matter whose height is higher (for n=15 particles, h_{mean}=84 ± 11 nm) than the one in the center of the RP. In addition, the deformation contrast is very high (~200 nm). These differences in deformation can be assimilated to in the composition of protein and lipid.

The confocal micrographs of LRP (Fig. 5, images D, E and F) show this arrangement of aggregated RP, with the presence of polar lipid dyes in the separation zones between RP (Fig. 5, image D), corresponding to the less deformable zones observed in AFM deformation images (Fig. 4, image E). It can be assumed that during particle aggregation, the membrane lipids remain present between the LRP and are linked to the *cis*-1,4-polyisoprene chains. But the membrane on top of the RP, exposed to a hydrophobic medium, might disrupt reaching a more stable configuration, forming lipid multilayers at the particle intersections. Image E (Fig. 5) also shows the spherical shapes of individual particles with hydrophobic *cis*-1,4-polyisoprene chains. This confirms that the *cis*-1,4-polyisoprene chains are not coalescing during adsorption of the LRP at the interface. The presence of lipids is also detected at the bottom of the sample, which, as observed on SRP deposits, confirms the presence of a continuous lipid background. After destructuration of the RP, the lipids displace to the air-liquid interface to form a stable amphiphilic monolayer.

The last type of structures observed in LRP films is shown in deformation and height modes on images F of Fig. 4 and Fig. 3, respectively. In height mode (image F, Fig. 3), crystal-like structures were observed around higher globules of micrometer size. Changing the color scale in image E of Fig. 3, as shown in insert framed with a red dotted line, highlighted the presence of those crystal-like structures in the background of the image, close to the LRP aggregate. In deformation mode (image F, Fig. 4), a smooth background is shown, as well as areas of stronger roughness, which seem to correspond to the center of the globules observed in image F, Fig. 3. The crystal-like structures are embedded in a low roughness zone. Nevertheless, after two days, these structures disappeared (data not shown) from the surface of the sample. They thus seem to be transient. Among the possible hypotheses, the crystal-like structures might be composed of pure lipids (neutral lipids, phospholipids, glycolipids, free fatty acids), pure proteins or *cis*-1,4-polyisoprene polymers. These assumptions are discussed below.

For RRIM600 clone, dry SRP and LRP fractions contain 4.27 and 1.78 % w/w of total lipids, respectively [26]. Total lipids mainly contain neutral lipids but also phospholipids and glycolipids. The profile of fatty acid chains of latex lipids from RRIM600 clone presents a majority of unsaturated chains containing at least one double bond C=C [64]. Phospholipids and glycolipids, wearing unsaturated acid chains, are in liquid expanded phases and cannot form condensed phases and participate in the crystal-like structure. One possibility would be the formation of crystal-like by neutral lipids, as observed by Anton and co-authors when spreading low density lipoprotein from egg yolk at the air-liquid interface [65]. Although our crystals do not display the same height and shape as the ones observed by Anton *et al.*, their formation could also be attributed to condensed phases of neutral lipids. Another possibility would be that the crystal-like structures originate from proteins, which represent 4.3 and 2.1 % w/w of dry SRP and LRP, respectively. However, the two most abundant proteins found in LRP and SRP fractions, SRPP1 and REF1, respectively [31], were subjected to several interfacial studies (alone [51] or interacting with synthetic [52] and native lipids [53]) but no crystalline structure has never been reported. Finally, the last possibility would be that the crystal-like structures are composed of *cis*-1,4-polyisoprene polymer, the main component of RP. Knowing the ability of *cis*-1,4-polyisoprene to crystalize under strain [66], it is believed that, during the interfacial film drying on mica, lateral forces induce transient crystallization around and on the top of the particle. This last possibility seems to us the most plausible. However, additional chemical identification technics would be required to confirm this assumption.

4. Conclusion

This work presents the first study of *Hevea brasiliensis* RP in their hydrated state at the air-liquid interface. RP were separated according to their size by centrifugation of freshly tapped ammonia-free latex from RRIM600 clone to obtain SRP and LRP. The combination of different techniques and, for the first time, confocal fluorescence microscopy enabled following the behavior of RP during the early coagulation steps. The main results demonstrate a greater stability of LRP by large lateral aggregation (several μm) at the interface preventing coalescence, even if the membrane appears altered. In contrast, SRP fuse rapidly losing their native morphology to form undefined and small aggregates (<μm) extruding membrane lipids, suggesting a lower lateral molecular cohesion in these particles. The anchoring in the RP membrane of the two major proteins, *i.e.* REF1 and SRPP1 whose concentration in SRP and LRP differs might be involved in the contrasted interfacial behaviors of RP.

The genotype being known as a strong variation factor of the biochemical composition of SRP and LRP [26], this work is going on with the investigation of clonal effect in the film formation process, as well as the characterization of the rheological properties of interfacial films. Our research contributes to a better understanding of the behavior

of SRP and LRP in their hydrated state and they could help to cope with the sustainability challenges of the concentrated latex industry. Indeed, huge quantities of sulfuric acid are required for coagulating skim (SRP suspended in C-serum) rubber to the detriment of the environment [23].

Abbreviations

RP, Rubber Particles; SRP, Small Rubber Particles; LRP, Large Rubber Particles; REF1, Rubber Elongation Factor; SRPP1, Small Rubber Particle Protein; NTA, Nanoparticles Tacking Analysis; AFM, Atomic Force Microscopy; BAM, Brewster Angle Microscopy; CLSM, Confocal Laser Scanning Microscopy.

CRediT authorship contribution statement

Véronique Vié: Writing – review & editing, Validation, Supervision, Project administration, Methodology, Funding acquisition, Conceptualization. **Siriluck Liengprayoon:** Validation, Supervision, Resources, Project administration. **Celine Bottier:** Writing – review & editing, Validation, Supervision, Project administration, Methodology, Funding acquisition, Conceptualization. **Gilles Paboeuf:** Validation, Supervision, Resources, Methodology, Data curation. **Natedao Musigamart:** Writing – review & editing, Resources, Project administration, Investigation. **Marion Baudoin:** Writing – original draft, Supervision, Project administration, Investigation, Formal analysis, Data curation.

Declaration of Competing Interest

The authors declare that they have no known competing financial interests or personal relationships that could have appeared to influence the work reported in this paper.

Data availability

Data will be made available on request.

Acknowledgments

We would like to thank Région Bretagne and CIRAD for funding the PhD grant of M. Baudoin, as well as Campus France, France (Ministères des Affaires Etrangères et de l'Enseignement Supérieur et de la Recherche) and OHEC, Thailand (Office of the Higher Education Commission, Thailand) for supporting the missions between France and Thailand (PHC SIAM, project N° 49493QB). We are very grateful to F. Gauffre for the NTA measurements, to B. Lefeuvre for the zeta potential measurements and to Visahakit Thai Rubber Co., Ltd. for kindly providing latex. We also would like to thank the MRic platform ('Microscopy Rennes Imaging Center', Rennes, France) for technical assistance with the confocal laser scanning microscope. Finally, the 2CBioMIF platform (ScanMAT-UAR 2025, Rennes, France) is acknowledged for allowing the biophysical characterization of the samples presented in this article. This work was undertaken as part of the Hevea Research Platform in Partnership (HRPP).

Appendix A. Supporting information

Supplementary data associated with this article can be found in the online version at doi:10.1016/j.colsurfb.2024.114281.

References

[1] R.S.B. IRSG, 78 (2023).
[2] C.K. John, S.Siew Weng, Accelerated auto-coagulation of skim latex, Rubb. Res. Inst. Malaya 23 (1973).
[3] J.L. Jacob, J.C. Prevôt, J. D'Auzac, The composition of natural latex from *Hevea brasiliensis*, Clin. Rev. Allergy 11 (1993) 325–337.
[4] P.B. Dickenson, Electron microscopical studies of latex vessel system of *Hevea brasiliensis*, J. Rubb. Res. Inst. Malaya 21 (1969) 543–559.
[5] J. D'Auzac, J.-L. Jacob, H. Chrestin, The composition of latex from Hevea brasiliensis as A laticiferous cytoplasm, Physiol. Rubber Tree Latex (1989) 56–96.
[6] C. Bottier, Biochemical composition of Hevea brasiliensis latex: A focus on the protein, lipid, carbohydrate and mineral contents, in: Advances in Botanical Research, Elsevier, 2020, pp. 201–237.
[7] L.N.S. Homans, J.W. Van Dalfen, G.E. van Gils, Complexity of fresh Hevea latex, Nature 161 (1948) 177–178.
[8] G.F.J. Moir, Ultracentrifugation and staining of hevea latex, Nature 184 (1959) 1626–1628.
[9] W.A. Southorn, Complex particles in Hevea latex, Nature 188 (1960) 165–166.
[10] K. Cornish, D.F. Wood, J.J. Windle, Rubber particles from four different species, examined by transmission electron microscopy and electron-paramagnetic-resonance spin labeling, are found to consist of a homogeneous rubber core enclosed by a contiguous, monolayer biomembrane, Planta 210 (1999) 85–96.
[11] K. Nawamawat, J.T. Sakdapipanich, C.C. Ho, Y. Ma, J. Song, J.G. Vancso, Surface nanostructure of The composition of natural latex from *Hevea brasiliensis* natural rubber latex particles, Colloids Surf. A: Physicochem. Eng. Asp. 390 (2011) 157–166.
[12] D.J. Siler, M. Goodrich-Tanrikulu, K. Cornish, A.E. Stafford, T.A. Mckeon, Composition of rubber particles of Hevea brasiliensis, Parthenium argentatum, Ficus elastica, and Euphorbia lactiflua indicates unconventional surface structure, Plant Physiol. Biochem. 35 (1997) 881–889.
[13] D.F. Wood, K. Cornish, Microstructure of purified rubber particles, Int. J. Plant Sci. 161 (2000) 435–445.
[14] G. De Oliveira Reis, T. Gibaud, B. Saint-Michel, S. Manneville, M. Leocmach, L. Vaysse, F. Bonfils, C. Sanchez, P. Menut, Irreversible hardening of a colloidal gel under shear: the smart response of natural rubber latex gels, J. Colloid Interface Sci. 539 (2019) 287–296.
[15] J.B. Gomez, S. Hamzah, Particle size distribution in Hevea latex-some observations on the electron microscopic method, J. Nat. Rubber Res. 4 (1989) 204–211.
[16] A.P. Singh, S.G. Wi, G.C. Chung, Y.S. Kim, H. Kang, The micromorphology and protein characterization of rubber particles in Ficus carica, Ficus benghalensis and Hevea brasiliensis, J. Exp. Bot. 54 (2003) 985–992.
[17] L. Tarachiwin, J.T. Sakdapipanich, Y. Tanaka, Relationship between particle size and molecular weight of rubber from *Hevea brasiliensis*, Rubber Chem. Technol. 78 (2005) 694–704.
[18] S. Yamashita, M. Mizuno, H. Hayashi, H. Yamaguchi, Y. Miyagi-Inoue, K. Fushihara, T. Koyama, T. Nakayama, S. Takahashi, Purification and characterization of small and large rubber particles from Hevea brasiliensis, Biosci., Biotechnol., Biochem. 82 (2018) 1011–1020.
[19] H.M. Lim, Colloidal and rheological properties of natural rubber latex concentrate, Appl. Rheol. 26 (2016) 15629.
[20] M. Sriring, A. Nimpaiboon, S. Kumarn, C. Sirisinha, J. Sakdapipanich, S. Toki, Viscoelastic and mechanical properties of large- and small-particle natural rubber before and after vulcanization, Polym. Test. 70 (2018) 127–134.
[21] S. Chaiprapat, S. Wongchana, S. Loykulnant, C. Kongkaew, B. Charnnok, Evaluating sulfuric acid reduction, substitution, and recovery to improve environmental performance and biogas productivity in rubber latex industry, Process Saf. Environ. Prot. 94 (2015) 420–429.
[22] S.T. Myint Maung, R. Kokoo, M. Khangkhamano, CO2 utilization for ammonia removal in skim latex: processing and rubber properties, Chem. Eng. Process. - Process. Intensif. 196 (2024) 109656.
[23] P. Dunuwila, V.H.L. Rodrigo, N. Goto, Improving financial and environmental sustainability in concentrated latex manufacture, J. Clean. Prod. 255 (2020) 120202.
[24] C. Tang, M. Yang, Y. Fang, Y. Luo, S. Gao, X. Xiao, Z. An, B. Zhou, B. Zhang, X. Tan, H.-Y. Yeang, Y. Qin, J. Yang, Q. Lin, H. Mei, P. Montoro, X. Long, J. Qi, Y. Hua, Z. He, et al., The rubber tree genome reveals new insights into rubber production and species adaptation, Nat. Plants 2 (2016) 1–10.
[25] Y.-C. Wei, D. Zhu, W.Y. Xie, J.H. Xia, M.F. He, S. Liao, In-situ observation of spatial organization of natural rubber latex particles and exploring the relationship between particle size and mechanical properties of natural rubber, Ind. Crops Prod. 180 (2022) 114737.
[26] S. Liengprayoon, L. Vaysse, S. Jantarasunthorn, K. Wadeesirisak, J. Chaiyut, S. Srisomboon, N. Musigamart, K. Rattanaporn, C. Char, F. Bonfils, C. Bottier, Distribution of the non-isoprene components in the four The composition of natural latex from *Hevea brasiliensis* latex centrifugation fractions, J. Rubber Res 24 (2021) 759–769.
[27] Q. Xiang, K. Xia, L. Dai, G. Kang, Y. Li, Z. Nie, C. Duan, R. Zeng, Proteome analysis of the large and the small rubber particles of *Hevea brasiliensis* using 2D-DIGE, Plant Physiol. Biochem. 60 (2012) 207–213.
[28] M.S. Dennis, D.R. Light, Rubber elongation factor from Hevea brasiliensis, J. Biol. Chem. 264 (1989) 18608–18617.
[29] S.K. Oh, H. Kang, D.H. Shin, J. Yang, K.-S. Chow, H.Y. Yeang, B. Wagner, H. Breiteneder, K.-H. Han, Isolation, characterization, and functional analysis of a novel cDNA clone encoding a small rubber Particle protein from The composition of natural latex from *Hevea brasiliensis*, J. Biol. Chem. 274 (1999) 17132–17138.
[30] H.Y. Yeang, K.F. Cheong, E. Sunderasan, et al., The 146 kd rubber elongation factor (Hev b 1) and 24 kd (Hev b 3) rubber particle proteins are recognized by IgE from patients with spina bifida and latex allergy, J. Allergy Clin. Immunol. 98 (1996) 628–639.
[31] K. Berthelot, S. Lecomte, Y. Estevez, F. Peruch, *Hevea brasiliensis* REF (Hev b 1) and SRPP (Hev b 3): an overview on rubber particle proteins, Biochimie 106 (2014) 1–9.

[32] S. Yamashita, H. Yamaguchi, T. Waki, Y. Aoki, M. Mizuno, F. Yanbe, T. Ishii, A. Funaki, Y. Tozawa, Y. Miyagi-Inoue, K. Fushihara, T. Nakayama, S. Takahashi, Identification and reconstitution of the rubber biosynthetic machinery on rubber particles from *Hevea brasiliensis*, eLife 5 (2016) e19022.
[33] K. Cornish, D.J. Scott, W. Xie, C.J.D. Mau, Y. Feng, X.-H. Liu, G.D. Prestwich, Unusual subunits are directly involved in binding substrates for natural rubber biosynthesis in multiple plant species, Phytochemistry 156 (2018) 55–72.
[34] M. Sriring, A. Nimpaiboon, N. Dechnarong, S. Kumarn, Y. Higaki, K. Kojio, A. Takahara, C.C. Ho, J. Sakdapipanich, Pre-vulcanization of large and small natural rubber latex particles: film-forming behavior and mechanical properties, Macromol. Mater. Eng. 304 (2019) 1900283.
[35] M. Sriring, A. Nimpaiboon, S. Kumarn, K. Higaki, Y. Higaki, K. Kojio, A. Takahara, C.C. Ho, J. Sakdapipanich, Film formation process of natural rubber latex particles: roles of the particle size and distribution of non-rubber species on film microstructure, Colloids Surf. A: Physicochem. Eng. Asp. 592 (2020) 124571.
[36] M. Sriring, Enhancing viscoelastic and mechanical performances of natural rubber through variation of large and small rubber particle combinations, Polym. Test. 81 (2020) 106225.
[37] S. He, F. Zhang, S. Liu, H. Cui, S. Chen, W. Peng, G. Chen, X. Liao, L. Liao, Influence of sizes of rubber particles in latex on mechanical properties of natural rubber filled with carbon black, Polymer 261 (2022) 125393.
[38] C Bottier, B. Gross, K. Wadeesirisak, S. Srisomboon, S. Jantarasunthorn, N. Musigamart, S. Roytrakul, S. Liengprayoon, L. Vaysse, P. Kunemann, M.-F. Vallat, K. Mougin, Rapid evolution of biochemical and physicochemical indicators of ammonia-stabilized Hevea latex during the first twelve days of storage, Colloids Surf. A: Physicochem. Eng. Asp. 570 (2019) 487–498.
[39] N. Payungwong, J. Sakdapipanich, J. Wu, C.-C. Ho, The interplay of protein hydrolysis and ammonia in the stability of hevea rubber latex during storage, Polymers 15 (2023) 4636.
[40] M.M. Rippel, L.-T. Lee, C.A.P. Leite, F. Galembeck, Skim and cream natural rubber particles: colloidal properties, coalescence and film formation, J. Colloid Interface Sci. 268 (2003) 330–340.
[41] K.B. Blodgett, Films built by depositing successive monomolecular layers on a solid surface, J. Am. Chem. Soc. 57 (1935) 1007–1022.
[42] W.G. Wren, Application of the Langmuir trough to the study of rubber latex, Trans. Rubber Ind. 16 (1941) 355–364.
[43] J.H. Clint, S.E. Taylor, Particle size and interparticle forces of overbased detergents: a langmuir trough study, Colloids Surf. 65 (1992) 61–67.
[44] J. Ruiz-Garcia, R. Gámez-Corrales, B.I. Ivlev, Foam and cluster structure formation by latex particles at the air/water interface, Phys. A: Stat. Mech. Its Appl. 236 (1997) 97–104.
[45] R. Aveyard, J.H. Clint, D. Nees, V.N. Paunov, Compression and structure of monolayers of charged latex particles at air/water and octane/water interfaces, Langmuir 16 (2000) 1969–1979.
[46] H. Scholtmeijer, The Langmuir-Blodgett behavior and film formation of methacrylate latex particle monolayers, PhD Thesis of University of Groningen, the Netherlands (2005).
[47] M. Deleu, J.-M. Crowet, M.N. Nasir, L. Lins, Complementary biophysical tools to investigate lipid specificity in the interaction between bioactive molecules and the plasma membrane: A review, BBA - Biomembr. 1838 (2014) 3171–3190.
[48] J. Sarkis, V. Vié, Biomimetic models to investigate membrane biophysics affecting lipid–protein interaction, Front. Bioeng. Biotechnol. 8 (2020) 270.
[49] C. Bottier, J. Géan, B. Desbat, A. Renault, D. Marion, Structure and orientation of puroindolines into wheat galactolipid monolayers, Langmuir 24 (2008) 10901–10909.
[50] E. Guzmán, F. Martínez-Pedrero, C. Calero, A. Maestro, F. Ortega, R.G. Rubio, A broad perspective to particle-laden fluid interfaces systems: from chemically homogeneous particles to active colloids, Adv. Colloid Interface Sci. 302 (2022) 102620.
[51] K. Berthelot, S. Lecomte, Y. Estevez, B. Coulary-Salin, F. Peruch, Homologous *Hevea brasiliensis* REF (Hevb1) and SRPP (Hevb3) present different auto-assembling, Biochim. Et. Biophys. Acta (BBA) - Proteins Proteom. 1844 (2014) 473–485.
[52] K. Berthelot, S. Lecomte, Y. Estevez, V. Zhendre, S. Henry, J. Thévenot, E. J. Dufourc, I.D. Alves, F. Peruch, Rubber particle proteins, HbREF and HbSRPP, show different interactions with model membranes, Biochim. Et. Biophys. Acta (BBA)-Biomembr. 1838 (2014) 287–299.
[53] K. Wadeesirisak, S. Castano, K. Berthelot, L. Vaysse, F. Bonfils, F. Peruch, K. Rattanaporn, S. Liengprayoon, S. Lecomte, C. Bottier, Rubber particle proteins REF1 and SRPP1 interact differently with native lipids extracted from *Hevea brasiliensis* latex, Biochim. Et. Biophys. Acta (BBA) - Biomembr. 1859 (2017) 201–210.
[54] M. Derde, F. Nau, V. Lechevalier, et al., Native lysozyme and dry-heated lysozyme interactions with membrane lipid monolayers: lateral reorganization of LPS monolayer, model of the Escherichia coli outer membrane, Biochim. Et. Biophys. Acta (BBA)-Biomembr. 1848 (2015) 174–183.
[55] C. Bourlieu, O. Ménard, A. De La Chevasnerie, L. Sams, F. Rousseau, M.-N. Madec, B. Robert, A. Deglaire, S. Pezennec, S. Bouhallab, F. Carrière, D. Dupont, The structure of infant formulas impacts their lipolysis, proteolysis and disintegration during in vitro gastric digestion, Food Chem. 182 (2015) 224–235.
[56] J. Kergomard, G. Paboeuf, N. Barouh, et al., Stability to oxidation and interfacial behavior at the air/water interface of minimally-processed versus processed walnut oil-bodies, Food Chem. 360 (2021) 129880.
[57] S. Bhattacharjee, DLS and zeta potential – what they are and what they are not? J. Control. Release 235 (2016) 337–351.
[58] J. Sansatsadeekul, J. Sakdapipanich, P. Rojruthai, Characterization of associated proteins and phospholipids in natural rubber latex, J. Biosci. Bioeng. 111 (2011) 628–634.
[59] C.C. Ho, T. Kondo, N. Muramatsu, H. Ohshima, Surface structure of natural rubber latex particles from electrophoretic mobility data, J. Colloid Interface Sci. 178 (1996) 442–445.
[60] W.W. Bowler, Electrophoretic mobility study of fresh hevea latex, Ind. Eng. Chem. 45 (1953) 1790–1794.
[61] V. Martinet, P. Saulnier, V. Beaumal, J.-L. Courthaudon, M. Anton, Surface properties of hen egg yolk low-density lipoproteins spread at the air–water interface, Colloids Surf. B: Biointerfaces 31 (2003) 185–194.
[62] J. Kergomard, G. Paboeuf, N. Barouh, P. Villeneuve, O. Schafer, T.J. Wooster, C. Bourlieu, V. Vié, Stability to oxidation and interfacial behavior at the air/water interface of minimally-processed versus processed walnut oil-bodies, Food Chem. 360 (2021) 129880.
[63] U. Sookmark, V. Pujade-Renaud, H. Chrestin, R. Lacote, C. Naiyanetr, M. Seguin, P. Romruensukharom, J. Narangajavana, Characterization of polypeptides accumulated in the latex cytosol of rubber trees affected by the tapping panel dryness syndrome, Plant Cell Physiol. 43 (2002) 1323–1333.
[64] S. Liengprayoon, J. Chaiyut, K. Sriroth, F. Bonfils, J. Sainte-Beuve, E. Dubreucq, L. Vaysse, Lipid compositions of latex and sheet rubber from the composition of natural latex from *Hevea brasiliensis*depend on clonal origin, Eur. J. Lipid Sci. Technol. 115 (2013) 1021–1031.
[65] S. Dauphas, V. Beaumal, P. Gunning, A. Mackie, P. Wilde, V. Vié, A. Riaublanc, M. Anton, Structures and rheological properties of hen egg yolk low density lipoprotein layers spread at the air–water interface at pH 3 and 7, Colloids Surf. B: Biointerfaces 57 (2007) 124–133.
[66] S. Toki, T. Fujimaki, M. Okuyama, Strain-induced crystallization of natural rubber as detected real-time by wide-angle X-ray diffraction technique, Polymer 41 (2000) 5423–5429.